Research in Pharmaceutical Sciences, April 2025; 20(2): 188-206
Received: 07-02-2024
Peer Reviewed:10-05-2024
Revised: 30-07-2024
Accepted: 20-08-2024
Published: 31-03-2025

School of Pharmacy & Pharmaceutical Sciences
Isfahan University of Medical Sciences

Original Article

Sodium oleate functionalized simvastatin liposomes: boosting endosomal escape and anticancer efficacy in triple negative breast cancer

Ebrahim Sadaqa[1], Satrialdi[1], Fransiska Kurniawan[2], and Diky Mudhakir[1,*]

[1]Department of Pharmaceutics, School of Pharmacy, Institut Teknologi Bandung (ITB), Bandung 40132, Indonesia.
[2]Department of Pharmacochemistry, School of Pharmacy, Institut Teknologi Bandung (ITB), Bandung 40132, Indonesia.

Abstract

Background and purpose: Due to delivery obstacles, Simvastatin, a potential anticancer agent, faces clinical limitations. This study aimed to enhance simvastatin delivery and efficacy against triple-negative breast cancer (TNBC) by developing liposomes modified with sodium oleate (NaOL) to improve endosomal escape.
Experimental approach: Simvastatin was encapsulated in 1,2-dimyristoyl-sn-glycero-3-phosphocholine/cholesterol liposomes through thin film hydration. Liposomes with poly(lactic-co-glycolic acid) (PLGA), individually modified with NaOL and PLGA, served as a control endosomal escape enhancer. Formulations were characterized for size, charge, and encapsulation efficiency. Endosomal escape was quantified through subcellular colocalization analysis using confocal microscopy, and anticancer activity was assessed by evaluating cytotoxicity against 4T1 TNBC cells, followed by measurements of intracellular reactive oxygen species (ROS) and DNA damage.
Findings/Results: Unmodified liposomes had a size of 115.2 ± 7.94 nm, a zeta potential of -9.67 ± 3.01 mV, and an encapsulation efficiency of 78.93% ± 6.72. NaOL-modified liposomes had a size of 119 ± 9.37 nm, a zeta potential of -31.05 ± 2.38 mV, and an encapsulation efficiency of 84.96% ± 2.51. While PLGA-modified liposomes had a size of 151.1 ± 7.35 nm, zeta potential of -18.68 ± 1.41 mV, and encapsulation efficiency of 83.63% ± 5.56. Importantly, NaOL-liposomes exhibited lower IC_{50} values, improved endosomal escape, and enhanced anticancer activity compared to unmodified liposomes.
Conclusion and Implications: Surface modification with NaOL is a promising strategy to enhance the anticancer efficacy of simvastatin liposomes against TNBC through improved endosomal escape. These encouraging *in-vitro* findings warrant further *in-vivo* investigations into the potential for NaOL-modified liposomes to improve TNBC patient outcomes.

Keywords: Endosomal escape; Liposomes; Simvastatin; Sodium oleate, Triple negative breast cancer.

INTRODUCTION

Triple-negative breast cancer (TNBC), which lacks expression of estrogen, progesterone, and human epidermal growth factor receptor 2 (HER2) receptors, accounts for 15-20% of breast cancer cases (1). Unlike receptor-positive subtypes, TNBC does not respond to endocrine or HER2-targeted therapies, presenting a major therapeutic challenge. TNBC is associated with younger age at diagnosis, higher tumor grade, increased metastatic risk, and poor prognosis. Due to the lack of approved targeted therapies, first-line treatment relies on cytotoxic chemotherapy. However, TNBC suffers from higher recurrence and relapse rates compared to other breast cancer subtypes. This aggressive clinical behavior, coupled with the lack of tailored targeted therapies, underscores the urgent need to identify innovative treatment strategies for managing TNBC (2).

*Corresponding author: D. Mudhakir
Tel: +62-222504852, Fax: +62-222504852
Email: mudhakir@itb.ac.id

Access this article online

Website: http://rps.mui.ac.ir

DOI: 10.4103/RPS.RPS_25_24

Cholesterol-lowering statins have recently displayed anticancer potential in preclinical models, including breast cancer. Simvastatin can induce cell apoptosis by inhibiting HMG-CoA reductase and the mevalonate pathway. Simvastatin depletes cells of essential isoprenoids that modify and activate pro-apoptotic proteins such as Rho, Rac, and Cdc42 (3,4). Additionally, simvastatin suppresses cancer-promoting signaling networks such as MAPK/ERK, PI3K/Akt, and Wnt/β-catenin, reducing proliferation, survival, and metastasis (5). Furthermore, simvastatin elevates intracellular reactive oxygen species (ROS), triggering p38/JNK activation and the apoptosis pathway (6,7). The multifaceted effects of simvastatin on tumor growth, survival, invasion, and oxidative stress highlight its potential utility as a breast cancer therapy.

However, realizing simvastatin's clinical potential has been hindered by its hydrophobicity and the high doses required for cancer treatment and prevention, which can lead to unintended side effects (8). Encapsulating simvastatin into nanocarriers presents a promising approach to overcoming these challenges by reducing the necessary dosage and enhancing targeted delivery, thereby minimizing toxicity and maximizing therapeutic efficacy (9). Liposomes have emerged as ideal carriers for hydrophobic drugs like simvastatin, improving pharmacokinetics and tumor accumulation through the enhanced permeability and retention effect (EPR) (10,11). Although enhanced penetration into tumors *via* the EPR effect is beneficial, the primary challenge remains to overcome intracellular sequestration within endo-lysosomal compartments. Following internalization into cancer cells, liposomes often become trapped within endosomes and are subsequently shuttled to lysosomes, where encapsulated drugs are degraded by lysosomal enzymes. This sequestration significantly limits the cytosolic release of therapeutics at target sites, drastically reducing their therapeutic efficacy (12). Therefore, strategies that promote escape from endo-lysosomal pathways are crucial for significantly improving drug delivery by enabling the release of therapeutics directly into the cytosol. Various approaches have been investigated to enhance endosomal escape, including cationic polymers, pH-sensitive lipids, and membrane-disruptive peptides, but have faced challenges such as toxicity, instability, and inadequate release (13). Engineering liposomes with optimized surfaces to enhance endosomal escape remains an important goal to elucidate the anticancer potential of nanomedicines against tumors.

Poly (lactic-co-glycolic acid) (PLGA), a biodegradable polymer known for its biocompatibility, biodegradability, and favorable release kinetics, has garnered attention as a drug delivery vehicle (14,15). PLGA nanotechnology revolutionizes delivery in oncology and other diseases by improving pharmacokinetics/dynamics, minimizing side effects, enhancing stability, prolonging release, and reducing dosing frequency (16). Importantly, PLGA nanoparticles can achieve rapid endo-lysosomal escape due to the selective reversal of their surface charge from anionic to cationic in acidic endo-lysosomal environments. This charge switch enables nanoparticle interaction with endo-lysosomal membranes, facilitating cytosolic escape where therapeutics can take effect (17). Therefore, this study utilized PLGA as a positive control biodegradable endosome escape enhancer.

Sodium oleate, a versatile salt of oleic acid, plays an important role in nanotechnology and drug delivery. Its affinity to form hydroxyl bonds with SiO_2 nanoparticles makes it a valuable asset for processes such as polymer flooding (18). Additionally, sodium oleate has been utilized to coat magnetic nanoparticles, thereby creating biocompatible stable colloids (19). As a surfactant and emulsifier, sodium oleate helps stabilize emulsions and micelles, which is valuable for drug encapsulation and delivery (20). While sodium oleate is known for enhancing the solubility and permeability of small molecules, specifically skin permeation, it has not yet been explored as an endosomal escape enhancer for nanoformulations.

This study aimed to investigate the potential of sodium oleate, when integrated into simvastatin liposomes, to facilitate endosomal escape safely and effectively following endocytosis in TNBC model cells *in vitro*. In addition, the impact of enhancing endosomal

escape on the anticancer efficacy of the therapeutic agents delivered was assessed. This in vitro study addresses a pivotal challenge in cancer nanotherapy and establishes a foundation for improved drug delivery systems in oncology. Additionally, it is expected to provide the impetus for subsequent *in vivo* investigations.

MATERIALS AND METHODS

Materials

The lipids 1,2-dimyristoyl-sn-glycero-3-phosphocholine (DMPC) and lipoid sodium oleate B were purchased from Lipoid GmbH (Ludwigshafen, Germany). Other materials obtained were: cholesterol, 4-(2-hydroxyethyl)-1-piperazineethanesulfonic acid (HEPES), and PLGA (lactide: glycolide 50:50) polymer from Sigma-Aldrich (St. Louis, MO, USA); phosphate-buffered saline (PBS), Dulbecco's modified Eagle's medium (high glucose DMEM), F12 nutrients, fetal bovine serum (FBS), penicillin-streptomycin, trypan blue, 0.25% trypsin solution, and trypsin-EDTA solution acquired from Gibco, Thermo Fisher Scientific (Waltham, MA, USA); and the fluorescent dyes LysoSensor Green DND-189 and Hoechst 33342 purchased from Thermo Fisher Scientific (Waltham, MA, USA).

Preparation of simvastatin-loaded liposomes

In this study, we prepared three types of liposomal formulations that contained simvastatin: simvastatin-loaded unmodified liposomes (Sim-Lipo), simvastatin-loaded PLGA liposome (Sim-PLGA-Lipo), and sodium oleate modified liposomes loaded with simvastatin (Sim-NaOL-Lipo). The unmodified liposomes contained a combination of DMPC phospholipid and cholesterol in a 9:1 molar ratio (0.005 mmol total phospholipid). The Sim-PLGA-Lipo formulation had the DMPC and cholesterol components but also included PLGA polymer at a concentration of 0.1% w/v. The Sim-NaOL-Lipo formulation was fabricated with DMPC, cholesterol, and sodium oleate in a 9:1:1 molar ratio (0.005 mmol total phospholipid, 10 mol% sodium oleate). All the liposomal formulations were prepared using the thin film hydration method as already described with modification (21). To briefly explain this method, the lipid components were dissolved in a solvent mixture containing chloroform and methanol in a 2:1 ratio. Simvastatin was then added to achieve an encapsulated drug concentration of 200 µg/mL at a drug-to-lipid molar ratio of 0.1. The organic solvents were removed under nitrogen flow to form a film, which was then hydrated using HEPES buffer (pH 7.2).

The resulting multilamellar liposomes were downsized by bath sonication at room temperature for 15 min to form unilamellar vesicles.

Physical characterization of simvastatin-loaded liposomes

The final formulation of simvastatin-loaded liposomes was characterized for its physical properties, which included size, polydispersity index, and zeta potential. Dynamic light scattering (DLS) was performed using a DelsaTM Nano C particle analyzer (Beckman Coulter, Brea, CA) to determine the liposome particle size and polydispersity index . The zeta potential was measured to evaluate the surface charge of the liposomes. Stability studies were conducted to detrmine the physical stability of the liposomes. All liposomal formulations were stored at 4 °C for 28 days. During this period, particle size, zeta potential, and polydispersity were measured periodically to assess any changes.

Entrapment efficiency percentage of simvastatin-loaded liposomes

The entrapment efficiency percentage of simvastatin-loaded liposomes was determined using the ultracentrifugation method, as previously described with some modifications (22). The liposomal dispersion was centrifuged at 20,000 rpm for 20 min at 4 °C. The supernatant was then collected, and the amount of encapsulated simvastatin was measured using a UV spectrophotometer at 238 nm. A calibration curve was prepared by measuring the absorbance of different concentrations of simvastatin. The concentration of encapsulated simvastatin was calculated based on the linear regression equation of the calibration curve.

The entrapment efficiency percentage was calculated using the following equation:

$$\text{Entrapment efficiency (\%)} = \frac{\textit{Encapsulated simvastatin concentration}}{\textit{Initial total simvastatin concentration}} \times 100$$

Morphology investigation

The shape of various prepared simvastatin liposomes was investigated using transmission electron microscopy (TEM). A Hitachi HT7700 TEM system (Tokyo, Japan) was used to conduct the analysis. To prepare the samples, the nanoparticle solutions were diluted with deionized water and pipetted directly onto carbon-coated copper grids before TEM imaging. TEM examination allowed to evaluate particle size distribution and morphological characterization of simvastatin liposome formulations.

Fourier-transform infrared spectroscopy

Fourier-transform infrared (FTIR) spectroscopy was performed to analyze the chemical composition and molecular interactions of various liposomal formulations using a Jasco FT/IR-4200 type A spectrometer (Jasco Corporation, Tokyo, Japan). The samples, including cholesterol, DMPC, DMPC-Chol Lipo, Sim-Lipo, NaOL, NaOL Lipo, Sim-NaOL-Lipo, PLGA, PLGA Lipo, and Sim-PLGA-Lipo, were mixed with potassium bromide (KBr) and compressed into pellets. Spectra were obtained over the range of 4000-400 cm^{-1}. The spectra were compared to identify characteristic absorption bands and analyze changes in functional groups andS molecular structure across different formulations.

4T1 cell culture

The 4T1 mouse mammary carcinoma cells (ATCC® CRL-2359) were obtained from Dr. Muhammad Hasan Bashari, Faculty of Medicine, Padjadjaran University, Indonesia. The cells were cultured in Dulbecco's modified eagle medium (DMEM) supplemented with 10% FBS. The cells were incubated at 37 °C in a humidified atmosphere with 5% CO_2. The culture medium was changed every 2-3 days, and the cells were passaged when they reached 80-90% confluency.

Cellular uptake

To evaluate the uptake mechanism of the developed liposomes, confocal laser scanning microscopy (CLSM) was utilized as described by Mudhakir *et al.* (23). Briefly, 2×10^5 of 4T1 breast cancer cells were cultured in glass-bottom 35 mm confocal dishes with standard DMEM growth medium. Before liposome treatment, cells were pretreated with endocytosis inhibitors, including hypertonic sucrose solution to inhibit clathrin-mediated endocytosis, amiloride to block micropinocytosis, and filipin as a caveolae-mediated inhibitor. Next, the unmodified, NaOL-modified, and PLGA liposomes loaded with the fluorescent marker DiD were incubated with the pretreated cells for 60 min at physiological conditions. After PBS washing, cell nuclei were labeled with Hoechst stain for visualization. Confocal microscopy was utilized to capture images and assess the cellular association of the DiD-liposomes under inhibitor conditions compared to control. Additionally, mean fluorescence intensity analysis using Image J software was conducted for semi-quantitative measurement of liposome uptake. This comprehensive approach, examining multiple mechanisms, will elucidate the predominant internalization pathway of the surface-modified simvastatin liposomes in the 4T1 TNBC cell line.

Assessment of endosome escape efficiency using subcellular colocalization analysis

Subcellular colocalization was conducted to evaluate the intracellular trafficking of different nanoformulations, as described by Hu *et al.* (24) with modification. Unmodified liposomes (Unmodified Lipo), sodium oleate-modified liposomes (NaOL Lipo), and PLGA-polymer-modified liposomes (PLGA Lipo) were prepared. The fluorescent membrane probe Vybrant DiD was incorporated into the lipid bilayers. 4T1 breast cancer cells were plated at 1×10^5 cells/well in glass-bottom 35 mm confocal dishes and grown for 24 h at 37 °C. The cells were then incubated with DiD-labeled liposomes for 1 h and 3 h. Post-incubation, LysoTracker Green DND-189 (100 nM) was applied for 30 min to fluorescently label

lysosomes, followed by Hoechst 33342 (1 µg/mL) for 10 min to stain nuclei. After washing three times with cold PBS, the cells were imaged using confocal laser scanning microscopy (Olympus FV-1200). Pearson's correlation coefficient was calculated using Fiji-ImageJ software to determine the colocalization between DiD-liposomes and LysoTracker in a semi-quantitative way as a measure of endosomal escape over time.

Cytotoxicity assessment

MTT colorimetric assay was conducted to evaluate the cytotoxic effects of simvastatin and its liposomal formulations on 4T1 mouse breast cancer cells. 4T1 cells were seeded in 96-well plates at a density of 5×10^3 cells per well in 100 µL of complete culture medium (DMEM supplemented with 10% FBS and 1% penicillin-streptomycin) and incubated overnight to allow adherence. Simvastatin was dissolved in methanol at 10 mg/mL and then diluted in serum-free DMEM to obtain working concentrations ranging from 0.781 to 100 µg/mL. The final methanol concentration in the dilutions was maintained below 1% to prevent potential cytotoxic effects. Empty liposomes and simvastatin-loaded liposomes (Sim-Lipo, Sim-NaOL-Lipo, and Sim-PLGA-Lipo) were diluted in serum-free DMEM to match the working concentration range of simvastatin (0.781-100 µg/mL). After 24 and 48 h of treatment, the medium containing the treatments was removed, and the cells were washed three times with PBS. Subsequently, 100 µL of MTT solution (0.5 mg/mL in serum-free DMEM) was added to each well, and the plates were incubated for 4 h at 37 °C. The resulting purple formazan crystals, indicative of metabolically active cells, were dissolved by adding 200 µL DMSO per well and incubating for 1 h at 37 °C. The absorbance was measured at 570 nm using a microplate reader. All experiments were performed in triplicate. The half-maximal inhibitory concentration (IC_{50}) values for each treatment were determined using CompuSyn software.

Evaluation of intracellular ROS production using DCF fluorescence

The non-fluorescent compound 2',7'-dichlorodihydrofluorescein diacetate (DCFH-DA) can permeate cell membranes. Inside the cell, DCFH-DA is hydrolyzed by esterases into 2',7'-dichlorodihydrofluorescein ($DCFH_2$) which is subsequently oxidized by ROS in the cell to generate the fluorescent molecule 2',7'-dichlorofluorescein (DCF). The fluorescence intensity of DCF is proportional to the intracellular ROS levels, allowing DCF to be utilized for evaluating ROS generation. To assess this, 4T1 cells were seeded in glass-bottom 35 mm confocal dishes at a density of 1×10^5 cells per well in 2 mL of complete medium. The cells were incubated overnight under humidified conditions at 37 °C with 5% CO_2. The 4T1 cells were treated with Sim-Lipo, Sim-NaOL-Lipo, and Sim-PLGA-Lipo at a concentration of 4 µg/mL in serum-free DMEM for 3 h. One confocal plate was left untreated (untreated cells) as a control. After washing twice with PBS to eliminate excess liposomes, the cells were incubated with 10 µM DCFH-DA for 40 min at 37 °C. The cells were washed twice more with PBS to remove any remaining fluorescence. Nuclei were stained with 1 µg/mL Hoechst 33342 for 10 min. Finally, the cells were visualized under a confocal laser scanning microscope (Olympus FV-1200). The intracellular ROS levels were assessed in a semi-quantitative way by calculating the mean fluorescence intensity for each sample utilizing ImageJ software.

Assessment of DNA single-strand breaks by fast halo assay

To evaluate DNA single-strand breaks (SSBs), the fast halo assay (FHA) was utilized. 4T1 cells were seeded at a density of 4.0×10^5 cells per well and allowed to incubate for 24 h at 37 °C in a 5% CO_2 atmosphere. Post incubation, the cells were exposed to 4 µg/mL of Sim-Lipo, Sim-NaOL-Lipo, and Sim-PLGA-Lipo for 2 h. Untreated cells were maintained as a negative control. After the treatments, cells were collected under dim light conditions to prevent DNA damage from light exposure. The cells were washed with cold PBS containing 5 mM EDTA and resuspended at 4.0×10^4 cells/100 µL in the same buffer. The cell suspension was mixed with an equal volume of prewarmed 2% low melting point agarose and then pipetted onto slides pre-coated with

1% normal melting point agarose. The slides were then placed on ice for at least 20 min to allow the agarose to solidify. Once solidified, the coverslips were gently removed, and the slides were incubated in the dark for 15 min in a solution of 300 mM NaOH. During the final 5 min of this incubation, 10 µg/mL ethidium bromide was added to stain the DNA. After incubation, the slides were rinsed with distilled water for 5 min to remove excess staining and buffer components. The slides were immediately analyzed under an inverted fluorescence microscope (Olympus IX73). For the assessment of DNA breakage, 50 cells per slide were examined, and nuclear diffusion factor (NDF) values were determined using HaloJ software (25).

Statistical analysis

All quantitative data were expressed as the mean ± SEM or SD. Each experiment was performed in duplicate or triplicate as stated. Statistical analyses were conducted using GraphPad Prism software version 8. Data distribution normality was confirmed with the Shapiro-Wilk test. Differences between groups were evaluated using one-way analysis of variance (ANOVA) followed by appropriate post-hoc analyses for multiple comparisons. Tukey's test was utilized for data sets with equal variances. For data sets with unequal variances, Kruskal-Wallis non-parametric testing was performed, accompanied by Dunn's post-test. *P* values less than 0.05 were considered statistically significant.

RESULTS

Characterization of simvastatin-loaded liposomes

According to the results, Sim-Lipo, Sim-NaOL-Lipo, and Sim-PLGA-Lipo were successfully formulated at a 200 µg/mL simvastatin concentration (Table 1). The polydispersity index (PDI) was under 0.5 for all formulations, denoting narrow size distributions without aggregation. The highly negative zeta potentials of Sim-NaOL-Lipo and Sim-PLGA-Lipo can be attributed to surface modification of the liposomes with anionic sodium oleate and PLGA polymer at physiological pH 7.2 (26,27). Liposomes are colloidal particles that form a stable dispersion in water with a small size. Therefore, when subjected to a centrifugal force, they remain in the supernatant. The free (unencapsulated) simvastatin, which has a larger size and density, precipitates at the bottom of the tube. A calibration curve was established for simvastatin at a wavelength of 238 nm. The equation of the line was $y = 0.005x - 0.0763$ ($R^2 = 0.9953$). Our results revealed good entrapment efficiency for all formulations. TEM further verified the spherical morphology and nanoscale dimensions of the liposomes (Fig. 1A). TEM micrographs revealed vesicular structures for all formulations with well-defined membranes and interior aqueous cores. Average sizes by TEM imaging aligned closely with DLS measurements. Stability studies conducted over 28 days highlighted the superior stability of Sim-NaOL-Lipo compared to the other formulations (Fig. 1B). Specifically, Sim-NaOL-Lipo maintained a stable particle size, starting at 119.0 ± 9.37 nm on day 1 and remaining consistent at 112.9 ± 6.54 nm on day 28, with a consistent PDI of about 0.25, and a slight decrease in zeta potential from -31.1 ± 2.4 mV to -23.6 ± 3.1 mV, reflecting excellent colloidal stability.

Table 1. Particle size, PDI, zeta potential, and entrapment efficiency of different simvastatin-loaded liposomes. Data are presented as mean ± SD, n = 3.

Groups	Particle size (nm)	PDI	Zeta potential (mV)	Entrapment efficiency (%)
Sim-Lipo	115.2 ± 7.9	0.201 ± 0.037	-9.67 ± 3.01	78.93% ± 6.72
Sim-NaOL-Lipo	119 ± 9.37	0.206 ± 0.011	-31.05 ± 2.38	84.96% ± 2.51
Sim-PLGA-Lipo	151.1 ± 7.35	0.245 ± 0.026	-18.68 ±1.41	83.63% ± 5.56

PDI, Polydispersity index; Sim-Lipo, simvastatin-loaded unmodified liposomes; Sim-NaOL-Lipo, simvastatin-loaded sodium oleate modified liposomes; Sim-PLGA-Lipo, simvastatin-loaded poly(dl-lactide-co-glycolide) modified liposomes.

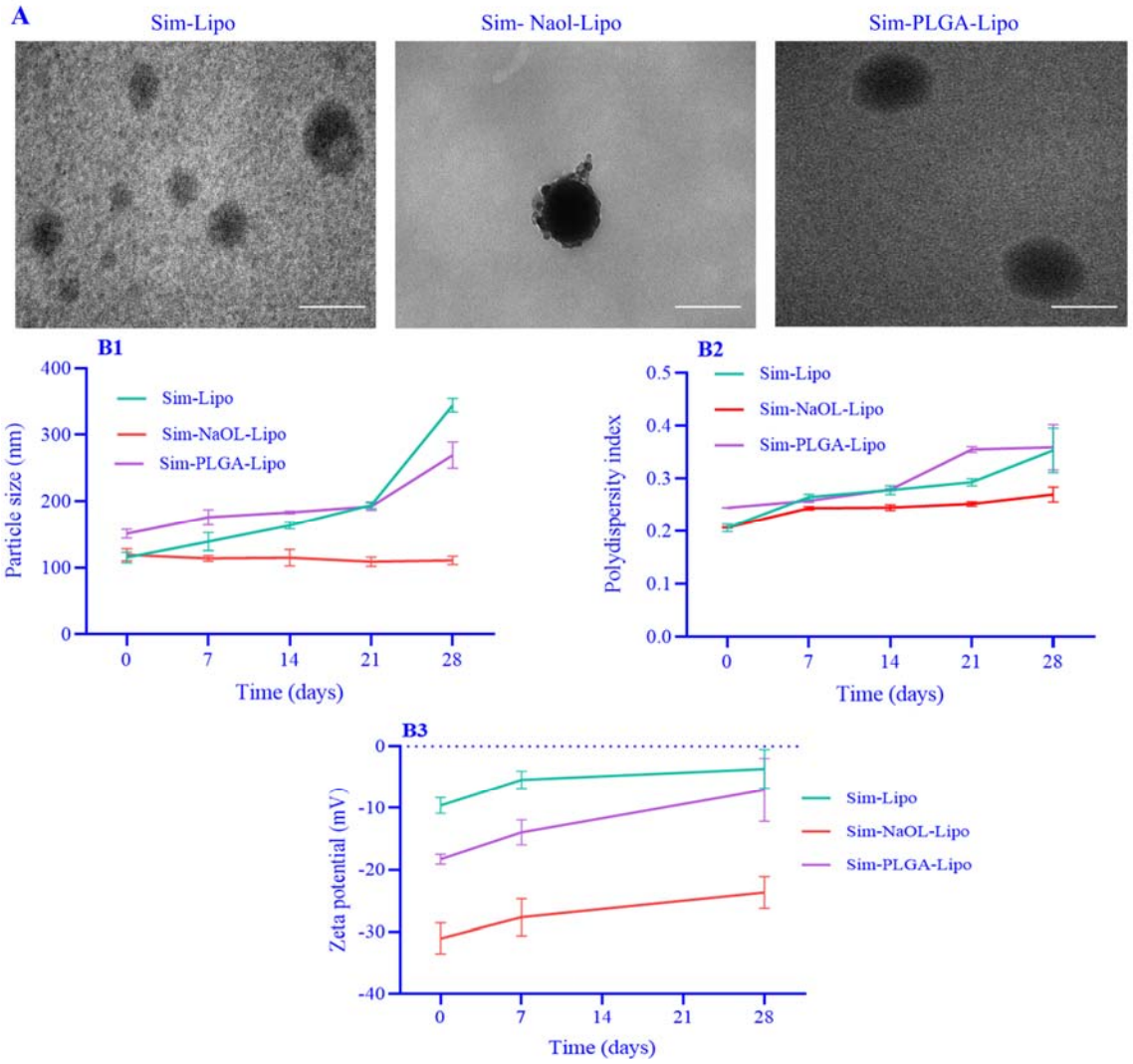

Fig. 1. (A) Transmission electron microscopy images. Scale bar: 200 nm. (B1-B3) Stability studies over 28 days. Sim-Lipo, simvastatin-loaded unmodified liposomes; Sim-NaOL-Lipo, simvastatin-loaded sodium oleate modified liposomes; Sim-PLGA-Lipo, simvastatin-loaded poly(dl-lactide-co-glycolide) modified liposomes.

FTIR Characterization

The FTIR spectra for the various liposomal formulations, highlighting characteristic absorption bands and molecular interactions, are presented in Fig. 2. As shown in Fig. 2A, the FTIR spectrum of DMPC-Chol Lipo displays characteristic absorption bands at 2954 cm^{-1} and 2870 cm^{-1}, attributed to the asymmetric and symmetric stretching vibrations of the CH_2 groups, respectively, indicative of lipid acyl chains (28). The absorption band at 1740 cm^{-1} corresponds to the C=O stretching vibration of ester carbonyl groups in the phospholipids. Bands at 1230 cm^{-1} and 1080 cm^{-1} are assigned to P=O and C-O stretching vibrations, respectively, typical for phospholipid bilayers (29). The FTIR spectrum of cholesterol exhibits a distinct peak at 1465 cm^{-1}, corresponding to CH_2 bending vibrations. This feature is consistent with the characteristic structure of cholesterol (30). The FTIR spectrum of Sim-Lipo (Fig. 2B) shows peaks at 2954 cm^{-1} and 2870 cm^{-1}, corresponding to CH_2 stretching vibrations, consistent with the lipid components seen in DMPC-Chol Lipo. The C=O stretching vibration of simvastatin

appears at around 1710 cm^{-1}, with no major or significant shift from its position in pure simvastatin. This minimal shift indicates that there are only minor interactions between simvastatin and the liposomal components, suggesting successful encapsulation. The bands at 1460 cm^{-1} and 1088 cm^{-1} correspond to CH_2 bending and C-O stretching vibrations, confirming the structural integrity of the liposomal formulation (31).

Figure 2C shows the spectrum of NaOL-Lipo, which exhibits characteristic peaks at 2925 cm^{-1} and 2855 cm^{-1}, attributed to CH_2 stretching vibrations. The band at 1560 cm^{-1} corresponds to the COO-asymmetric stretching vibration, indicating the presence of sodium oleate. The absorption band at 1420 cm^{-1} is assigned to the COO-symmetric stretching vibration. These peaks are consistent with the spectrum of NaOL, confirming its incorporation into the liposomal formulation (32). The DMPC-Chol Lipo spectrum remains consistent with its characteristic peaks, indicating successful modification of the liposomes with NaOL.

The FTIR spectrum of Sim-NaOL-Lipo (Fig. 2D) demonstrates notable peaks at 2954 cm^{-1} and 2870 cm^{-1}, corresponding to CH_2 stretching vibrations. The C=O stretching vibration of simvastatin appears at around 1710 cm^{-1}, with no major or significant shift compared to its position in pure simvastatin. This minimal shift indicates only minor interactions between simvastatin and the NaOL-modified liposomal components, suggesting successful encapsulation. The bands at 1460 cm^{-1} and 1088 cm^{-1} correspond to CH_2 bending and C-O stretching vibrations, confirming the structural integrity of the NaOL liposomes.

In Fig. 2E, the spectrum of PLGA Lipo displays characteristic peaks at 1750 cm^{-1}, attributed to the C=O stretching vibration of PLGA (33). Bands at 2935 cm^{-1} and 2850 cm^{-1} correspond to CH_2 stretching vibrations. The presence of PLGA in the liposomal formulation was confirmed by the absorption bands at 1460 cm^{-1} and 1088 cm^{-1}, assigned to CH_2 bending and C-O stretching vibrations, respectively. The FTIR spectrum of Sim-PLGA-Lipo (Fig. 2F) shows peaks at 2954 cm^{-1} and 2850 cm^{-1}, corresponding to CH_2 stretching vibrations. The C=O stretching vibration of simvastatin appeared at around 1710 cm^{-1}, confirming the successful encapsulation of simvastatin into the PLGA-modified liposomal components (34). The FTIR analysis confirmed the successful encapsulation and interaction of simvastatin with various liposomal components, indicating the effectiveness of the formulations in incorporating the drug. The presence of sodium oleate and PLGA modifications in the liposomal structures was validated through characteristic peak shifts and additional absorption bands, demonstrating the structural and compositional integrity of the modified liposomes.

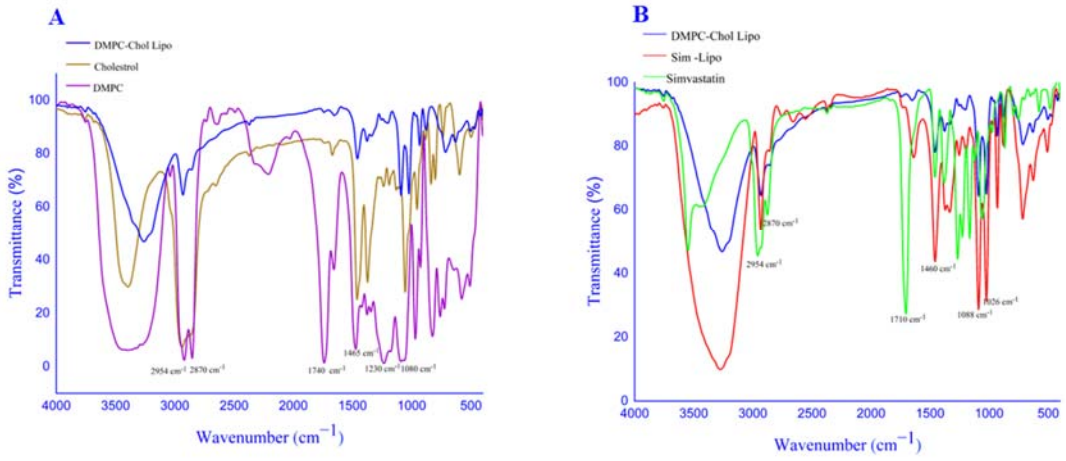

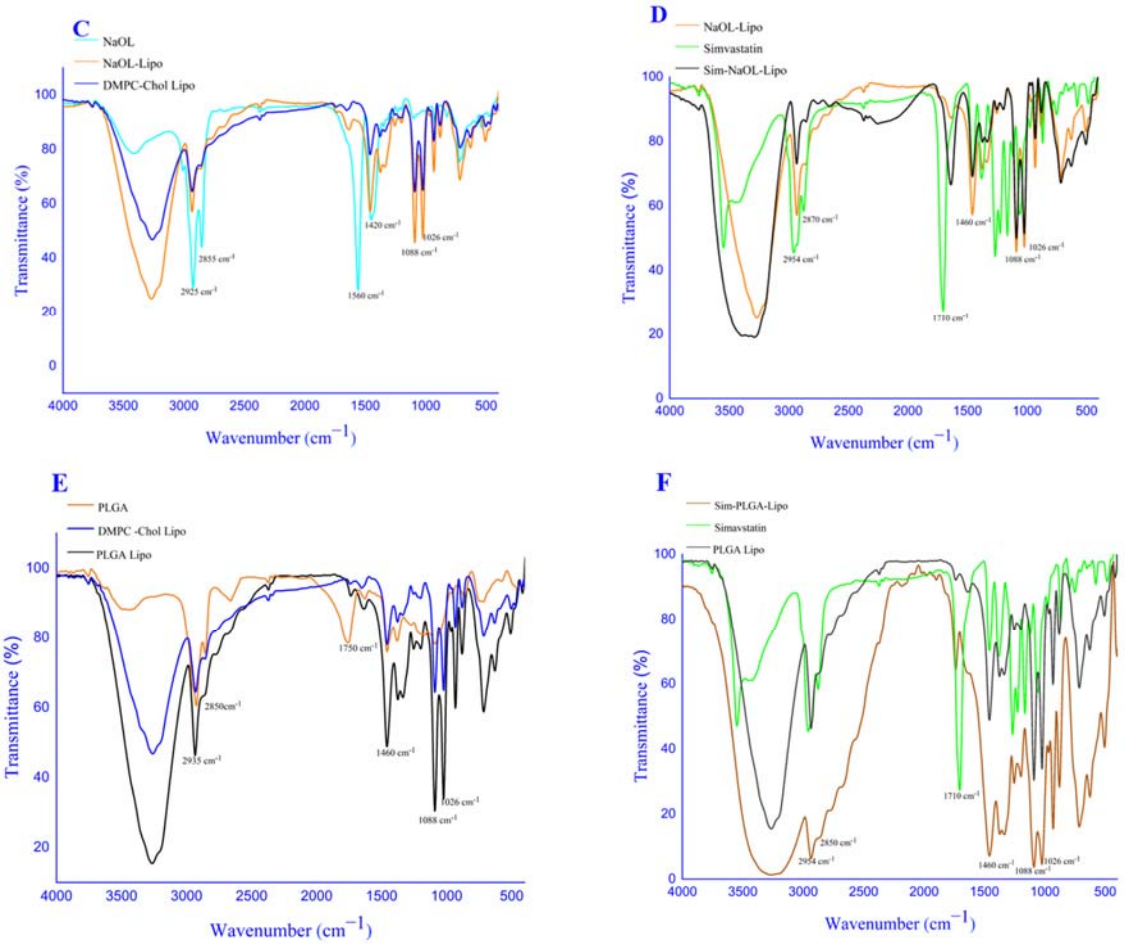

Fig. 2. FTIR spectra of various liposomal formulations and their components. Overlays are shown for (A) DMPC, cholesterol, and DMPC-Chol Lipo; (B) simvastatin, DMPC-Chol Lipo, and Sim-Lipo; (C) NaOL, DMPC-Chol Lipo, and NaOL-Lipo; (D) simvastatin, NaOL-Lipo, and Sim-NaOL-Lipo; (E) PLGA, DMPC-Chol Lipo, and PLGA-Lipo; (F) simvastatin, PLGA-Lipo, and Sim-PLGA-Lipo. DMPC, 1,2-Dimyristoyl-sn-glycero-3-phosphocholine; Sim-Lipo, simvastatin-loaded unmodified liposomes; Sim-NaOL-Lipo, simvastatin-loaded sodium oleate modified liposomes; Sim-PLGA-Lipo, simvastatin-loaded poly(lactide-co-glycolide) modified liposomes; Chol Lipo; cholesterol liposomes.

Cellular uptake

Cellular uptake studies employing endocytosis inhibitors elucidated the predominant internalization mechanisms of unmodified and surface-modified liposomes in 4T1 TNBC cells through confocal imaging. Uptake was quantified by mean fluorescence intensity calculations in a semi-quantitative manner using ImageJ software. Unmodified liposomes displayed significant uptake *via* both clathrin-mediated endocytosis (73% reduction by hypertonic sucrose) and caveolae-mediated endocytosis (55% reduction by filipin), and non-significant macropinocytosis (11% reduction by amiloride, $P = 0.115$) as shown in Fig. 3A. In contrast, sodium oleate incorporation into liposomes significantly promoted a major dependence on caveolae-mediated trafficking (74% reduction by filipin) and macropinocytosis (49% reduction by amiloride). Hypertonic sucrose pre-treatment did not significantly reduce NaOL liposome uptake (13.5% reduction by hypertonic sucrose, $P = 0.745$), indicating minimal involvement of the clathrin route (Fig. 3B). In contrast, PLGA liposomes displayed predominant uptake through clathrin-mediated endocytosis (66% reduction by hypertonic sucrose), as well as macropinocytosis (21% reduction by amiloride, $P = 0.018$). Non-significant reduction was observed with filipin (13% reduction by filipin, with a P-value of 0.581), denoting minimal contribution of the caveolae pathway (Fig. 3C).

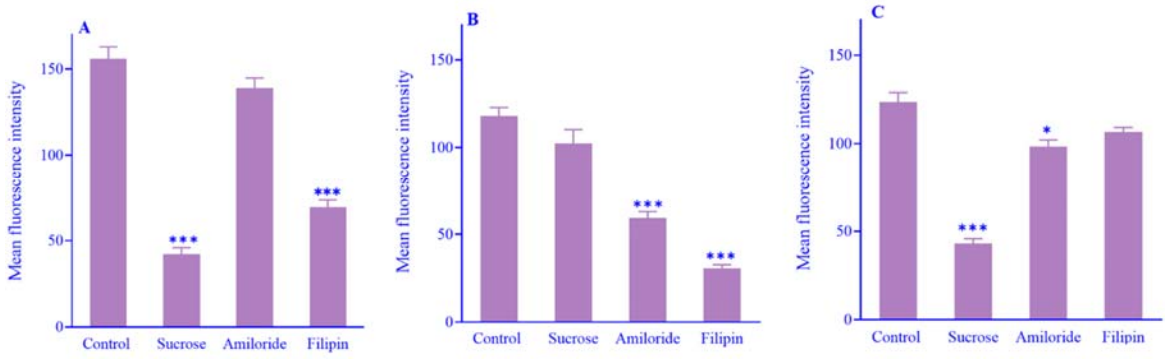

Fig. 3. Comparison of mean fluorescence intensities indicating cellular uptake across treatment groups after a 60-min incubation. The histogram presents data for (A) unmodified liposomes, (B) NaOL liposomes, and (C) PLGA liposomes. Measurement of fluorescence intensity was performed using ImageJ software. The data reflect the mean ± SEM based on three independent experiments, representing an analysis of 20 cells per sample. *$P < 0.05$ and ***$P < 0.001$ indicate significant differences in comparison with the control group (untreated cells). NaOL, Sodium oleate; PLGA, poly(lactide-co-glycolide).

Endosomal escape efficiency

The efficiency of endosomal escape for various liposome formulations was investigated using semiquantitative subcellular colocalization analysis. This analysis compared the escape capabilities of NaOL Lipo and PLGA Lipo against unmodified Lipo controls. Representative images of subcellular localization are shown in Fig. 4A. Remarkably, after just 1 h of incubation, the NaOL Lipo and PLGA Lipo formulations exhibited statistically significantly enhanced escape from the endolysosomal compartment compared to unmodified liposomes, as evidenced by lower Pearson's correlation coefficient values indicating reduced colocalization of the modified liposomes with lysosomes (Fig. 4B). Moreover, analysis at 3 hours post-incubation revealed persistently and profoundly improved escape for both NaOL Lipo and PLGA Lipo formulations relative to unmodified liposomes. Representative images at 3 h illustrate this effect (Fig. 4C), highlighting the continued cytosolic presence of modified liposomes. This observation is further supported by Pearson's correlation coefficient values, which reflect the decreased colocalization of NaOL Lipo and PLGA Lipo with lysosomes (Fig. 4D). The remarkable persistence of this effect across both early and late time points underscores the robust, sustained nature of the cytosolic access unlocked by our nanoparticle surface modifications.

Cytotoxic effects against 4T1 breast cancer cells

Our cytotoxicity data revealed a promising anticancer potential for liposome-formulated simvastatin against metastatic 4T1 TNBC cells. Both free simvastatin and nano-encapsulated simvastatin reduced cell viability in a concentration-dependent manner after 24 h of treatment, as shown in Fig. 5A. However, the liposomal preparations demonstrated markedly enhanced potency compared to the free simvastatin solution. Notably, the IC_{50} value of standard liposomal simvastatin (Sim-Lipo) at 26.9 ± 8.05 µg/mL was nearly 1.4 times lower than free simvastatin at 37.7 ± 3.81 µg/mL. Surface modification with sodium oleate (Sim-NaOL-Lipo) further reduced the IC_{50} over 2.9-fold to 9.1 ± 4.58 µg/mL compared to conventional liposomes. Furthermore, modification with a PLGA coating (Sim-PLGA-Lipo) enhanced cytotoxicity relative to standard liposomes with an IC_{50} of 12.9 ± 4 µg/mL. Importantly, blank liposomes showed high cell viability across the tested concentration range (Fig.5B). This confirms the cytocompatibility of the nanocarriers and demonstrates that the observed cytotoxic effects of the simvastatin formulations can be attributed to the drug itself.

Extending the incubation period to 48 h provided further insights into the cytotoxicity profiles of the formulations (Fig. 5C).

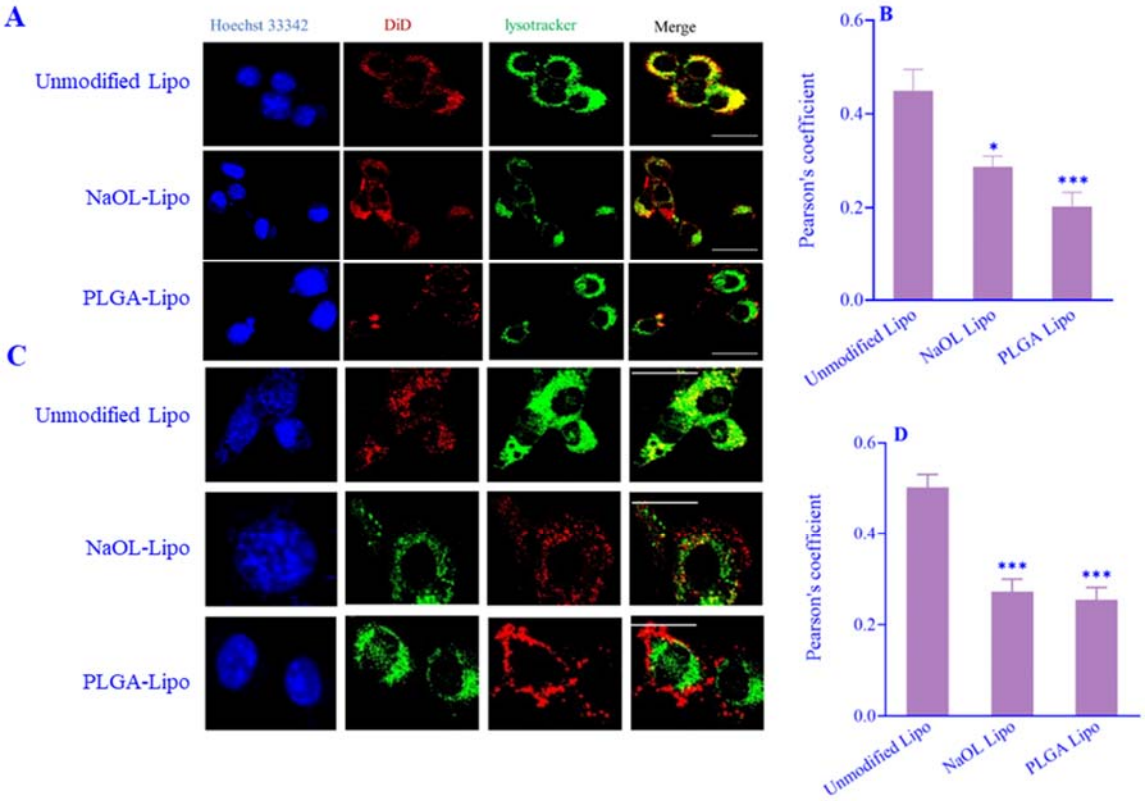

Fig. 4. Assessment of endosomal escape efficiency by subcellular colocalization analysis. 4T1 cells were incubated with DiD-labeled unmodified liposomes, NaOL-Lipo, and PLGA-Lipo for (A and B) 1 and (C and D) 3 h. Confocal microscopy images show intracellular trafficking of DiD-labeled liposomes (red fluorescence) relative to LysoTracker-stained endosomes/lysosomes (green fluorescence) and Hoechst 33342-counterstained nuclei (blue fluorescence). The bar indicates 100 µm. Quantitative colocalization analysis between the red (liposomes) and green (lysosomes) channels was performed using Pearson's correlation coefficients in Fiji-ImageJ software. Data are expressed as mean ± SEM of three independent experiments. ***$P < 0.001$ indicates significant differences in comparison with unmodified liposomes.

The IC_{50} values after 48 h of treatment were calculated as follows: simvastatin at 34.21 ± 2.45 µg/mL, Sim-NaOL Lipo at 8.7 ±1.81 µg/mL, Sim-PLGA Lipo at 11.70 ± 3.28 µg/mL, and Sim-Lipo at 21.91± 5.03 µg/mL. These results indicate a general trend of increased potency with extended exposure, highlighting the enhanced cytotoxic effects over a longer period. The moderate decrease in IC_{50} values from 24 to 48 h suggests a consistent and sustained cytotoxic activity, reflecting the effective anticancer activity of the formulations over time. Additionally, blank liposomes showed high cell viability across the tested concentration range after 48 h (Fig. 5D), confirming the cytocompatibility of the nanocarriers. Overall, these results demonstrate that modifying simvastatin liposomes with sodium oleate significantly enhanced the cytotoxic efficacy of simvastatin, with sustained effects over longer incubation periods. This highlights the potential of surface modifications in improving drug delivery and therapeutic outcomes in cancer treatment.

Intracellular ROS levels

Our analysis of reactive oxygen species production revealed valuable insights into the intracellular delivery capabilities of the nanoformulations. Sim-NaOL-Lipo and PLGA-Lipo stimulated markedly elevated DCF fluorescence intensity relative to the untreated control cells and standard unmodified Sim-Lipo, indicative of heightened ROS generation. In contrast, the unmodified liposomes failed to provoke ROS activity beyond baseline untreated levels ($P = 0.475$), as shown in Fig. 6A and B.

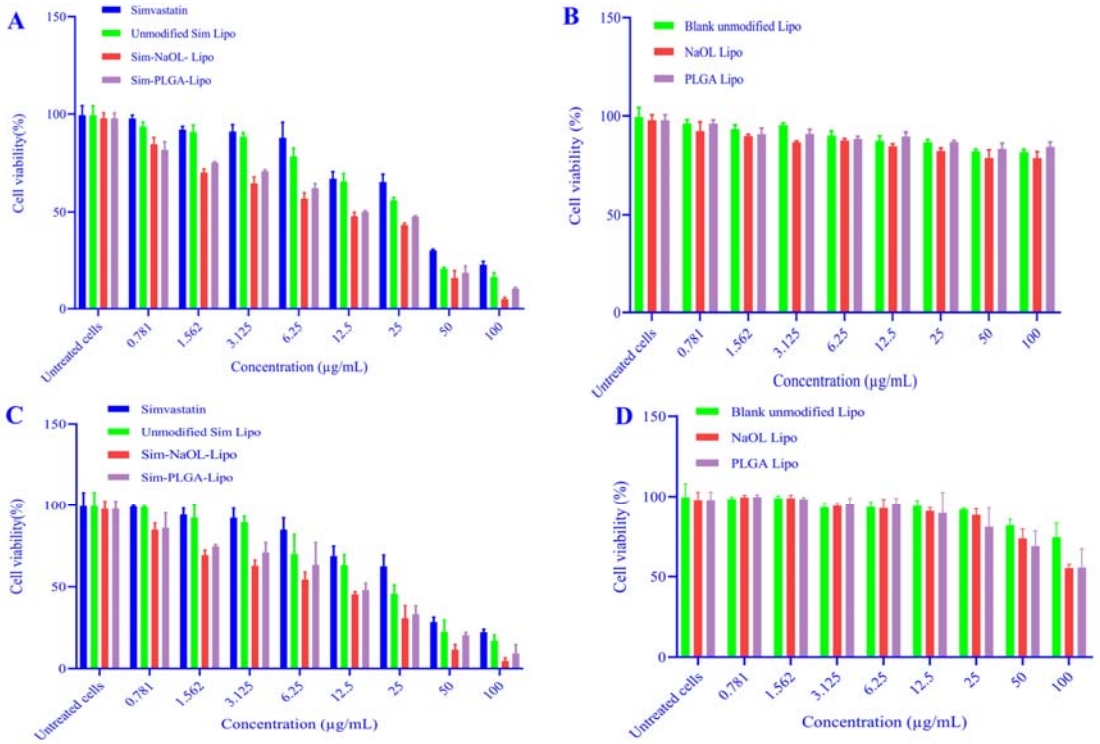

Fig. 5. Percentage of 4T1 cell viability after 24 and 48 h of treatment with simvastatin formulations, measured by MTT assay. Effects of simvastatin, Sim-Lipo, Sim-NaOL-Lipo, Sim-PLGA-Lipo, and blank liposome on 4T1 cell viability after (A and B) 24 h and (C and D) 48 h treatment. Data are presented as mean ± SD, n = 3. Sim-Lipo, simvastatin-loaded unmodified liposomes; Sim-NaOL-Lipo, simvastatin-loaded sodium oleate modified liposomes; Sim-PLGA-Lipo, simvastatin-loaded poly(lactide-co-glycolide) modified liposomes.

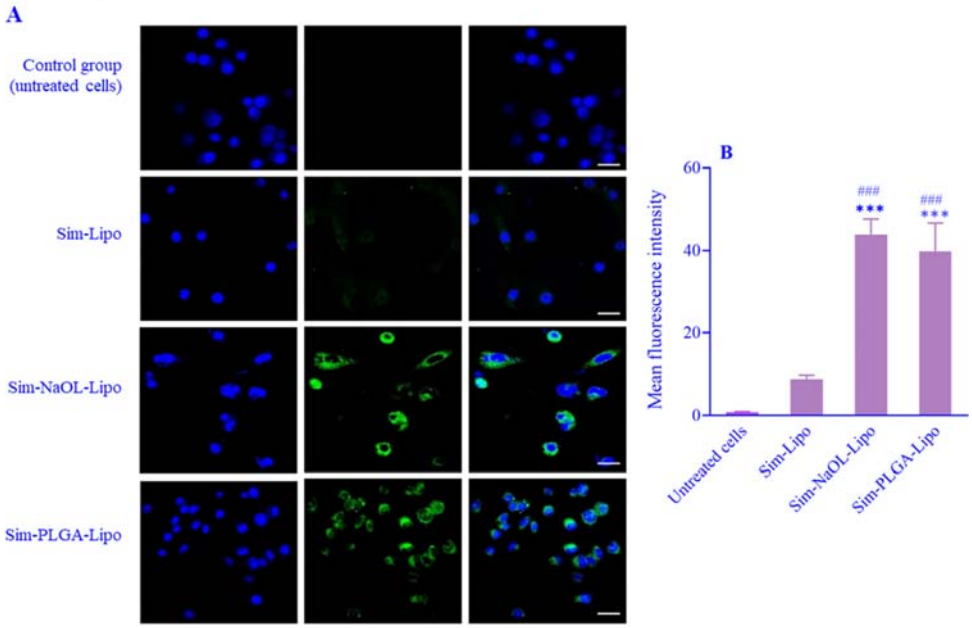

Fig. 6. Intracellular reactive oxygen species levels in 4T1 cells after treatment with simvastatin-loaded liposomes. (A) Confocal images showing DCF fluorescence (green) and Hoechst nuclear staining (blue) in untreated 4T1 cells as well as cells treated for 3 h with Sim-Lipo, Sim-NaOL-Lipo, and Sim-PLGA-Lipo at 4 μg/mL. The bar indicates 50 μm. (B) Histogram of upregulation of DCF fluorescence. The results are shown as mean ± SEM of two separate studies, n = 20. ***$P < 0.001$ indicates significant differences in comparison with the control group (untreated cells); $^{###}P < 0.001$ versus Sim-Lipo. Sim-Lipo, simvastatin-loaded unmodified liposomes; Sim-NaOL-Lipo, simvastatin-loaded sodium oleate modified liposomes; Sim-PLGA-Lipo, simvastatin-loaded poly(lactide-co-glycolide) modified liposomes.

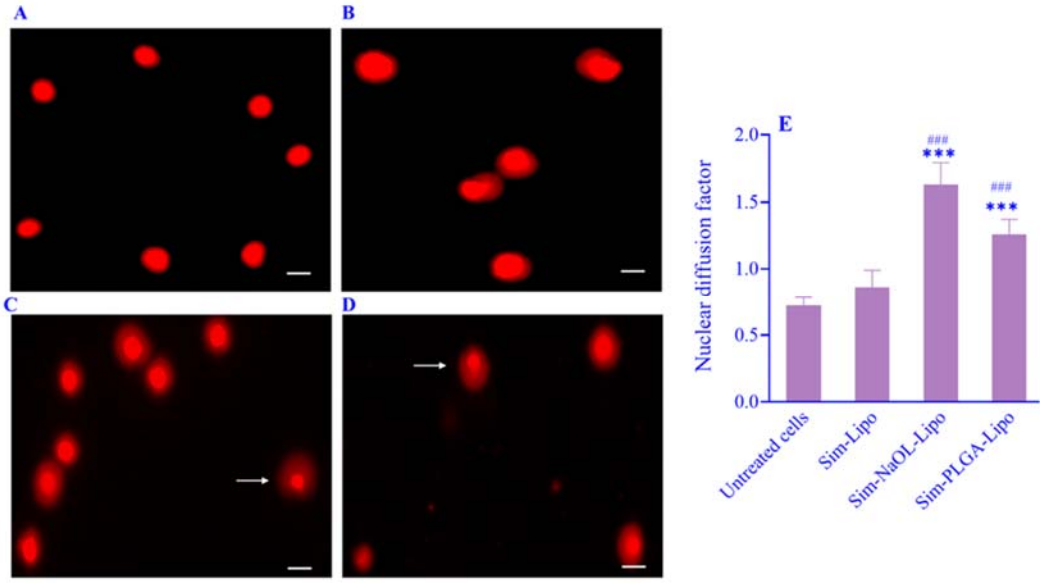

Fig. 7. DNA single-strand break analysis in 4T1 cells by fast halo assay. Representative fluorescence microscopy images of 4T1 cells treated with simvastatin-loaded liposomes and analyzed using an inverted microscope Olympus IX73. (A) Untreated cells (control). (B) Cells treated with 4 µg/mL Sim-Lipo. (C) Cells treated with 4 µg/mL Sim-NaOL-Lipo. (D) Cells treated with 4 µg/mL Sim-PLGA-Lipo. Single-stranded DNA was stained with ethidium bromide. Scale bar = 10 µm. (E) Histogram showing DNA damage level as quantified by nuclear diffusion factor from several randomly selected microscope images. Results are presented as mean ± SEM of three independent experiments, n = 50. ***$P < 0.001$ indicates significant differences in comparison with the control group (untreated cells); $^{###}P < 0.001$ versus unmodified Sim-Lipo. Sim-Lipo, simvastatin-loaded unmodified liposomes; Sim-NaOL-Lipo, simvastatin-loaded sodium oleate modified liposomes; Sim-PLGA-Lipo, simvastatin-loaded poly(lactide-co-glycolide) modified liposomes.

Assessment of DNA damage

The FHA determines DNA SSBs through semi-quantitative fluorescence analysis, with higher NDF values indicating greater DNA fragmentation. Without exposure, 4T1 breast cancer cells displayed limited basal DNA disruption (low control NDF). Incubation with unmodified Sim-Lipo did not significantly alter this baseline genomic stability profile ($P > 0.99$ *vs.* control). Conversely, surface-engineered liposomes Sim-NaoL-Lipo provoked considerably amplified DNA strand severing compared to untreated cells and native liposome formulations based on elevated NDF metrics from halo plots (Fig. 7A-D). Similarly, modified liposomes with PLGA polymer (Sim-PLGA-Lipo) elicited marked genomic fracturing compared to the control and unmodified counterparts according to heightened fragmentation indices (Fig. 7E)

DISCUSSION

This study demonstrated the promising potential of engineered simvastatin liposomes as an innovative therapeutic strategy against metastatic TNBC. Surface modification with NaOL enhanced the anticancer efficacy of liposome-encapsulated simvastatin against 4T1 cells by promoting endosomal escape and augmenting intracellular delivery. Notably, this represents the first application of NaOL as a safe biosurfactant capable of enhancing the endosomal release of therapeutic nanoparticles, thereby improving anticancer efficacy.

Mechanistic studies provided insights into how the formulations differed in cellular trafficking. Unmodified DMPC: Cholesterol liposomes displayed uptake *via* clathrin-mediated endocytosis and caveolae pathways. This aligns with evidence that under normal conditions, clathrin-mediated endocytosis facilitates the uptake of DMPC: DMPG (7:3 molar ratio) liposomes by human coronary artery endothelial cells. However, under inflammatory conditions resembling the tumor microenvironment, uptake can increase through clathrin-mediated routes (35). In contrast, the integration of sodium oleate markedly shifted dependence toward caveolae and

macropinocytosis pathways. This agrees with the findings that oleate modulates membrane properties, including lipid rafts and fluidity. Previous work revealed cellular uptake of sodium oleate nanoemulsions in MDCKII cells, controlled by specific caveolae-dependent endocytosis (36). PLGA promotion of uptake mainly through clathrin-mediated endocytosis and partial macropinocytosis is consistent with known cellular entry mechanisms for PLGA nanoparticles. Previous research revealed clathrin-mediated endocytosis as the primary pathway for PLGA nanoparticle internalization into human glioblastoma cells (37). Critically, sodium oleate and PLGA enabled statistically significant, sustained endosomal escape over 3 h versus unmodified liposomes. This establishes the value of surface engineering with sodium oleate for unlocking cytosolic drug release to engage intracellular targets rather than lysosomal degradation.

Building on the enhanced intracellular access, our cytotoxicity data then revealed markedly greater potency for the nanoformulations over free drugs, consistent with previous evidence that liposomal carriers can increase the bioavailability and antitumor effects of hydrophobic agents like simvastatin (38,39). Importantly, blank liposomes showed no toxicity, confirming the cytocompatibility of the phospholipid, cholesterol, PLGA, and sodium oleate nanocarriers (40-42). This suggests the cytotoxic effects resulted from the drug, not the delivery system. Notably, sodium oleate and PLGA integration further enhanced cytotoxicity compared to standard liposomes. Moreover, previous work has validated specialized endosomolytic nanoparticles that facilitate timely endolysosomal escape to trigger amplified therapeutic effects by evading clearance and allowing cargo diffusion into deeper cellular compartments (43). This signifies that surface engineering strategies can build on the inherent advantages of nano-encapsulation to further optimize therapeutic outcomes.

To assess downstream anticancer effects following endosomal escape, we examined validated mechanisms of simvastatin-induced apoptosis, including ROS generation and DNA damage (44,45). Simvastatin can stimulate apoptosis by Akt and NF-kB downregulation coupled with upregulating nitric oxide and ROS levels, causing eventual DNA fragmentation (46,47). Accordingly, the sodium oleate and PLGA-modified liposomes stimulated substantially increased ROS generation compared to native liposomes, confirming successful endosomal escape-enabled intracellular simvastatin bioactivity. Similarly, only the modified liposomes created marked DNA damage, evidencing enhanced nuclear delivery of simvastatin to destabilize cancer cell genomes through these known apoptosis pathways. In contrast, the unmodified formulation failed to impact genomic dysfunction or ROS levels.

As depicted in Fig. 8 we propose a model in which sodium oleate enhances endosomal escape through a pH-triggered mechanism involving targeted membrane fusion and integration events. Sodium oleate, an anionic biosurfactant, has an amphiphilic structure with a hydrophobic oleic acid tail and a hydrophilic carboxylate headgroup, which facilitates its incorporation into lipid membranes. Under acidic endosomal conditions (pH around 5), the carboxylate group of sodium oleate protonates, converting it into neutral oleic acid. This protonation increases the molecule's hydrophobicity, enhancing its insertion into lipid bilayers. Previous reports have suggested that an 18-carbon monounsaturated acyl chain with a central cis double bond, as found in oleic acid, elicits potent reorganizing and destabilizing effects on lipid bilayers (48). This membrane destabilization capacity relates to the distinct kinked molecular geometry of oleic acid conferred by its cis double bond, which drives increased fluidity and reduced order within the inserted bilayer (49,50). As previously demonstrated, oleic acid readily integrates into lipid bilayers, wherein it acts as a potent fusogen through mechanisms including classical stalk-mediated merging and stabilization of non-lamellar phases (51-53). In our proposed mechanism, upon entry into the acidic environment of the endosome, sodium oleate undergoes protonation, transforming into neutral oleic acid. This transformation significantly increases the molecule's hydrophobicity, enabling the oleic acid to

integrate seamlessly into the endosomal membrane. The hydrophobic tail of oleic acid embeds itself deeply within the lipid bilayer core, while the hydrophilic carboxyl moiety aligns at the aqueous interface. This strategic positioning not only induces membrane curvature but also increases the membrane's fluidity, a critical factor in destabilizing the bilayer structure.

The heightened fluidity, combined with the unique kinked structure of oleic acid, disrupts the orderly arrangement of lipid molecules, thereby facilitating the formation of a stalk-like intermediate. This stalk formation represents a crucial initial step in the fusion process between the liposomal and endolysosomal membranes. As the process progresses, the stalk evolves into an early fusion pore, which expands into a more mature late pore. This late pore serves as a gateway, enabling the efficient release of encapsulated liposomal cargo directly into the cytoplasm.

Supporting studies by Torchilin *et al*. have shown that pH-sensitive liposomes containing phosphatidylethanolamine, oleic acid, and cholesterol can fuse with standard liposomes under acidic conditions, leading to cargo mixing and enhanced permeability (54). This demonstrates oleic acid's inherent ability to promote membrane fusion and cargo release when included in an optimized lipid formulation. Consequently, sodium oleate is suggested to achieve pH-triggered, targeted endosomal escape through oleic acid-mediated membrane fusion and surfactant integration, leveraging its amphiphilic nature.

The increased hydrophobicity and fluidity of oleic acid under acidic conditions contribute significantly to this process. However, the full elucidation of this mechanism might require further investigation, particularly to understand the molecular interactions and dynamics involved.

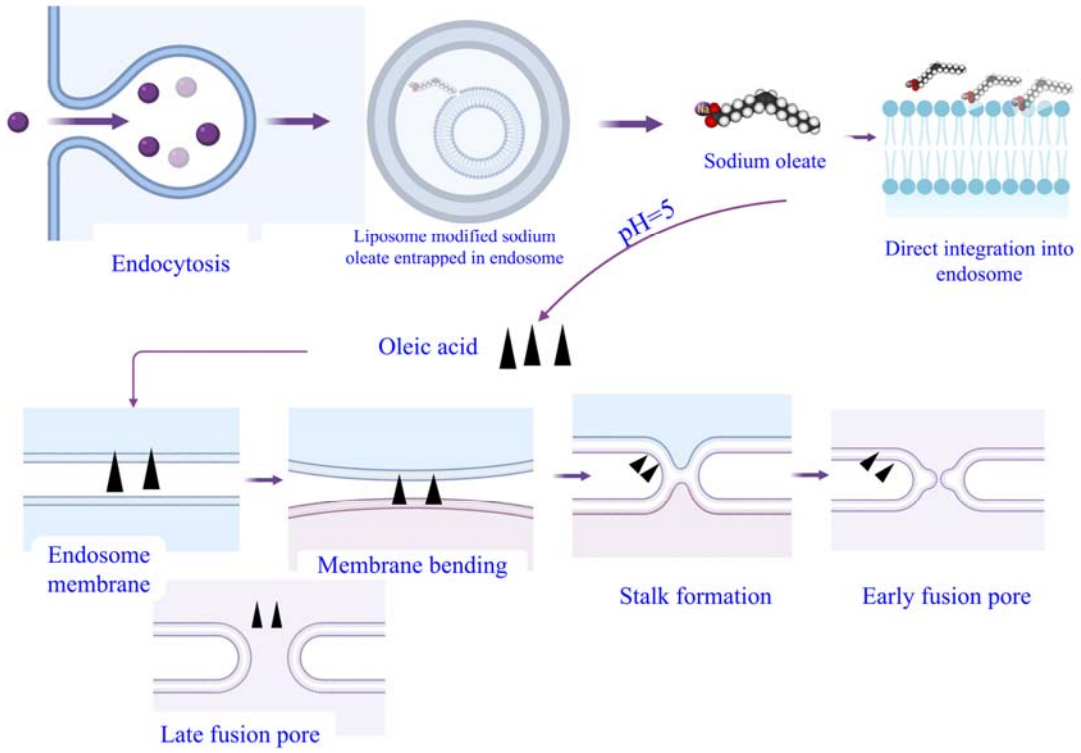

Fig. 8. Proposed mechanism of potential endosomal escape facilitated by surface modification with sodium oleate.

Despite our robust *in-vitro* results, providing a strong foundation for understanding the benefits of NaOL-modified liposomes, these findings highlight the substantial therapeutic gains achievable through this novel modification. To further build upon these encouraging results, additional *in-vivo* investigations are imperative. Such studies will yield critical insights into the efficacy and potential toxicity of these formulations within a more complex biological context. Furthermore, *in vivo* studies are essential for a comprehensive evaluation of pharmacokinetics and biodistribution profiles, which are crucial for the clinical translation of these promising formulations. Future investigations should aim to elucidate the specific pathways and molecular interactions that facilitate the enhanced endosomal escape and intracellular delivery observed with NaOL-modified simvastatin liposomes. A deeper understanding of these mechanisms will be pivotal in optimizing the formulation for maximal therapeutic benefit. By conducting these additional *in-vivo* studies, we can effectively translate our promising *in-vitro* findings into clinical applications. This could significantly advance the development of NaOL-modified liposomes as a viable therapeutic option for TNBC. Furthermore, the modification technique using sodium oleate holds potential for broader application, enhancing anticancer activity against other malignancies and representing a significant advancement in nanotechnology-based drug delivery.

CONCLUSION

In summary, this study indicated that sodium oleate-modified simvastatin liposomes significantly enhance the delivery and anticancer efficacy of simvastatin in treating metastatic TNBC. The modifications improved endosomal escape and intracellular release of simvastatin, leading to increased cytotoxicity, ROS generation, and DNA damage in TNBC cells compared to unmodified liposomes. These promising *in-vitro* findings lay a solid foundation for the future development and clinical translation of sodium oleate-modified nanocarriers, potentially offering a more effective treatment option for TNBC.

Acknowledgments

This work was partially supported by sincere thanks to the School of Pharmacy at ITB Community Service and Innovation Research Grant (SF.PPMI-1-14-2023) from Institut Teknologi Bandung, Indonesia. We sincerely thank the School of Pharmacy at ITB for their steadfast assistance during our research and publication efforts. We also appreciate the ITB Nanoscience and Nanotechnology Research Center (PPNN) and the ITB-Olympus Bioimaging Center (IOBC) for granting us access to their cutting-edge equipment, such as the FV1200 confocal laser scanning microscope from Olympus Life Science. Furthermore, we extend our sincere appreciation to Dr. Muhammad Hasan Bashari from the Faculty of Medicine, Padjadjaran University, Indonesia, for kindly providing the 4T1 mouse mammary carcinoma cells used in this study.

Conflict of interest statement

The authors declared no conflict of interest in this study.

Author's contributions

E. Sadaqa contributed to the conceptualization, methodology, data curation, original draft preparation, and editing the article; Satrialdi provided supervision, conducted data analysis and visualization, and contributed to review and editing the article; F. Kurniawan offered supervision and conducted investigation and visualization; and D. Mudhakir contributed to conceptualization, supervision, project administration, and review and editing the article. All authors read and approved the finalized article.

REFERENCES

1. Baranova A, Krasnoselskyi M, Starikov V, Kartashov S, Zhulkevych I, Vlasenko V, *et al*. Triple-negative breast cancer: current treatment strategies and factors of negative prognosis. J Med Life. 2022;15(2):153-161.
DOI: 10.25122/jml-2021-0108.

2. Yin L, Duan JJ, Bian XW, Yu SC. Triple-negative breast cancer molecular subtyping and treatment progress. Breast Cancer Res. 2020;22(1):61,1-13. DOI: 10.1186/s13058-020-01296-5.
3. Watson R, Tulk A, Erdrich J. The link between statins and breast cancer in mouse models: a systematic review. Cureus. 2022;14(11):e31893,1-12. DOI: 10.7759/cureus.31893.
4. Alizadeh J, Zeki AA, Mirzaei N, Tewary S, Rezaei Moghadam A, Glogowska A, *et al*. Mevalonate cascade inhibition by simvastatin induces the intrinsic apoptosis pathway *via* depletion of isoprenoids in tumor cells. Sci Rep. 2017;7:44841,1-14. DOI:10.1038/srep44841.
5. Wang T, Seah S, Loh X, Chan CW, Hartman M, Goh BC, *et al*. Simvastatin-induced breast cancer cell death and deactivation of PI3K/Akt and MAPK/ERK signalling are reversed by metabolic products of the mevalonate pathway. Oncotarget. 2016;7(3):2532-2544. DOI: 10.18632/oncotarget.6304.
6. Bai F, Yu Z, Gao X, Gong J, Fan L, Liu F. Simvastatin induces breast cancer cell death through oxidative stress up-regulating miR-140-5p. Aging (Albany NY). 2019;11(10):3198-3219. DOI: 10.18632/aging.101974.
7. Shen YY, Yuan Y, Du YY, Pan YY. Molecular mechanism underlying the anticancer effect of simvastatin on MDA-MB-231 human breast cancer cells. Mol Med Rep. 2015;12(1):623-630. DOI: 10.3892/mmr.2015.3411.
8. Licarete E, Sesarman A, Banciu M. Exploitation of pleiotropic actions of statins by using tumour-targeted delivery systems. J. Microencapsul. 2015;32(7):619-631. DOI: 10.3109/02652048.2015.1073383.
9. Askarizadeh A, Butler AE, Badiee A, Sahebkar A. Liposomal nanocarriers for statins:a pharmacokinetic and pharmacodynamics appraisal. J Cell Physiol 2019;234(2):1219-1229. DOI: 10.1002/jcp.27121.
10. Chen LC, Chang CH, Yu CY, Chang YJ, Hsu WC, Ho CL, *et al*. Biodistribution, pharmacokinetics and imaging of 188Re-BMEDA-labeled pegylated liposomes after intraperitoneal injection in a C26 colon carcinoma ascites mouse model. Nucl. Med. Biol. 2007;34(4):415-423. DOI: 10.1016/j.nucmedbio.2007.02.003.
11. Stapleton S, Milosevic M, Allen C, Zheng J, Dunne M, Yeung I, *et al*. A mathematical model of the enhanced permeability and retention effect for liposome transport in solid tumors. PLoS One. 2013;8(12):e81157,1-10. DOI: 10.1371/journal.pone.0081157.
12. Qiu C, Xia F, Zhang J, Shi Q, Meng Y, Wang C, *et al*. Advanced strategies for overcoming endosomal/lysosomal barrier in nanodrug delivery. Res. 2023;6:0148,1-23. DOI: 10.34133/research.0148.
13. Pei D, Buyanova M. Overcoming endosomal entrapment in drug delivery. Bioconjug. Chem. 2018;30(2):273-283. DOI: 10.1021/acs.bioconjchem.8b00778.
14. Ciocîlteu MV, Podgoreanu P, Delcaru C, Chifiriuc MC, Manda CV, Biță A, *et al*. PLGA-gentamicin biocomposite materials with potential antimicrobial applications in orthopedics. Farmacia. 2019;67(4):580-586. DOI: 10.31925/farmacia.2019.4.4.
15. Postelnicu RA, Ciocîlteu MV, Neacşu IA, Nicolicescu C, Costachi A, Amzoiu M, *et al*. PLGA-bisphosphonates conjugated nanoparticles:Synthesis and morphological characterization. Farmacia. 2023;71(1):83-90. DOI: 10.31925/farmacia.2023.1.11.
16. Beach MA, Nayanathara U, Gao Y, Zhang C, Xiong Y, Wang Y, *et al*. Polymeric nanoparticles for drug delivery. Chem Rev. 2024;124(9):5505-5616. DOI: 10.1021/acs.chemrev.3c00705.
17. Panyam J, Zhou W, Prabha S, Sahoo SK, Labhasetwar V. Rapid endo-lysosomal escape of poly(DL-lactide-co-glycolide) nanoparticles:Implications for drug and gene delivery. FASEB J. 2002;16(10):1217-1226. DOI: 10.1096/fj.02-0088com.
18. Llanos S, Giraldo LJ, Santamaria O, Franco CA, Cortés FB. Effect of sodium oleate surfactant concentration grafted onto SiO2 nanoparticles in polymer flooding processes. ACS Omega. 2018;3(12):18673-18684. DOI: 10.1021/acsomega.8b02944.
19. Roth HC, Schwaminger S, Fraga García P, Ritscher J, Berensmeier S. Oleate coating of iron oxide nanoparticles in aqueous systems: the role of temperature and surfactant concentration. J Nanopart Res. 2016;18(99):1-12. DOI: 10.1007/s11051-016-3405-2.
20. Walde P, Ichikawa S. Lipid vesicles and other polymolecular aggregates:from basic studies of polar lipids to innovative applications. Appl. Sci. 2021;11(21):10345,1-81. DOI: 10.3390/app112110345.
21. Predut D, Semenescu AD, Manea A, Dinu S, Popovici R, Jivanescu A. Cytotoxicity assessment of liposomes loaded with biologically active substances on oral tumour cells. Farmacia. 2022;70(6):1081-1088. DOI: 10.31925/farmacia.2022.6.11.
22. Khafagy ES, Almutairy BK, Abu Lila AS. Tailoring of novel bile salt stabilized vesicles for enhanced transdermal delivery of simvastatin: a new therapeutic approach against inflammation. Polymers (Basel). 2023;15(3):677,1-18. DOI: 10.3390/polym15030677.
23. Mudhakir D, Akita H, Harashima H. Topology of octaarginines (R8) or IRQ ligand on liposomes affects the contribution of macropinocytosis- and caveolae-mediated cellular uptake. React Funct Polym. 2011;71(3):340-343. DOI: 10.1016/j.reactfunctpolym.2010.11.013.
24. Hu Q, Wang Y, Xu L, Chen D, Cheng L. Transferrin conjugated pH- and redox-responsive poly(amidoamine) dendrimer conjugate as an efficient drug delivery carrier for cancer therapy. Int J Nanomedicine. 2020;15: 2751-2764. DOI: 10.2147/IJN.S238536.

25. Maurya DK. HaloJ:an imageJ program for semiautomatic quantification of DNA damage at single-cell level. Int J Toxicol. 2014;33(5):362-366. DOI: 10.1177/1091581814549961.
26. Araújo-Neto RP, Silva-Freitas EL, Carvalho JF, Pontes TRF, Silva KL, Damasceno IHM, *et al*. Monodisperse sodium oleate coated magnetite high susceptibility nanoparticles for hyperthermia applications. J Magn Magn Mater. 2014;364:72-79. DOI: 10.1016/j.jmmm.2014.04.001.
27. Platel A, Carpentier R, Becart E, Mordacq G, Betbeder D, Nesslany F. Influence of the surface charge of PLGA nanoparticles on their in *vitro* genotoxicity, cytotoxicity, ROS production, and endocytosis. J Appl Toxicol. 2016;36(3):434-444. DOI: 10.1002/jat.3247.
28. Briuglia ML, Rotella C, McFarlane A, Lamprou DA. Influence of cholesterol on liposome stability and on *in vitro* drug release. Drug Deliv Transl Res. 2015;5(3):231-242. DOI: 10.1007/s13346-015-0220-8.
29. Yonar D, Sünnetçioğlu MM. Spectroscopic and calorimetric studies on trazodone hydrochloride-phosphatidylcholine liposome interactions in the presence and absence of cholesterol. Biochim Biophys Acta. 2014;1838(10):2369-2379. DOI: 10.1016/j.bbamem.2014.06.009.
30. Ali I, Rehman J, Ullah S, Imran M, Javed I, El-Haj BM, *et al*. Preliminary investigation of novel tetra-tailed macrocycle amphiphile based nano-vesicles for amphotericin B improved oral pharmacokinetics. Artif Cells Nanomed Biotechnol. 2018;46(sup3):1204-1214. DOI: 10.1080/21691401.2018.1536061.
31. Brito Raj S, Chandrasekhar KB, Reddy KB. Formulation, *in-vitro* and *in-vivo* pharmacokinetic evaluation of simvastatin nanostructured lipid carrier loaded transdermal drug delivery system. Futur J Pharm Sci. 2019;5(1):1-14. DOI: 10.1186/s43094-019-0008-7.
32. Zhou X, Wang J, Wu J, Yang X, Yung BC, Lee LJ, *et al*. Preparation and evaluation of a novel liposomal formulation of cisplatin. Eur J Pharm Sci. 2015;66:90-95. DOI: 10.1016/j.ejps.2014.10.004.
33. Shaker MN, Ramadan HS, Mohamed MM, El khatib AM, Roston GD. Enhanced photodynamic efficacy of PLGA-encapsulated 5-ALA nanoparticles in mice bearing Ehrlich ascites carcinoma. Appl Nanosci. 2014;4:777-789. DOI: 10.1007/s13204-013-0268-z.
34. Nath SD, Son S, Sadiasa A, Min YK, Lee BT. Preparation and characterization of PLGA microspheres by the electrospraying method for delivering simvastatin for bone regeneration. Int J Pharm. 2013;443(1-2):87-94. DOI: 10.1016/j.ijpharm.2012.12.037.
35. Zhaorigetu S, Rodriguez-Aguayo C, Sood AK, Lopez-Berestein G, Walton BL. Delivery of negatively charged liposomes into the atherosclerotic plaque of apolipoprotein E-deficient mouse aortic tissue. J Liposome Res. 2014;24(3):182-190. DOI: 10.3109/08982104.2013.863208.
36. Dong D, Quan E, Yuan X, Xie Q, Li Z, Wu B. Sodium oleate-based nanoemulsion enhances oral absorption of chrysin through inhibition of UGT-mediated metabolism. Mol Pharm. 2017;14(9):2864-2874. DOI: 10.1021/acs.molpharmaceut.6b00851.
37. Malinovskaya Y, Melnikov P, Baklaushev V, Gabashvili A, Osipova N, Mantrov S, *et al*. Delivery of doxorubicin-loaded PLGA nanoparticles into U87 human glioblastoma cells. Int J Pharm. 2017;524(1-2):77-90. DOI: 10.1016/j.ijpharm.2017.03.049.
38. Luput L, Sesarman A, Porfire A, Achim M, Muntean D, Casian T, *et al*. Liposomal simvastatin sensitizes C26 murine colon carcinoma to the antitumor effects of liposomal 5-fluorouracil *in vivo*. Cancer Sci. 2020;111(4):1344-1356. DOI: 10.1111/cas.14312.
39. El Sabeh M, Vincent KL, Afrin S, Motamedi M, Saada J, Yang J, *et al*. Simvastatin-loaded liposome nanoparticles treatment for uterine leiomyoma in a patient-derived xenograft mouse model: a pilot study. J Obstet Gynaecol. 2022;42(6):2139-2143. DOI: 10.1080/01443615.2022.2033964.
40. Nikpoor AR, Jaafari MR, Zamani P, Teymouri M, Gouklani H, Saburi E, *et al*. Cell cytotoxicity, immunostimulatory and antitumor effects of lipid content of liposomal delivery platforms in cancer immunotherapies: a comprehensive *in vivo* and *in vitro* study. Int J Pharm. 2019;567:118492,1-9. DOI: 10.1016/j.ijpharm.2019.118492.
41. Sun J, Zhou S, Hou P, Yang Y, Weng J, Li X, *et al*. Synthesis and characterization of biocompatible Fe3O4 nanoparticles. J Biomed Mater Res A. 2007;80(2):333-341. DOI: 10.1002/jbm.a.30909.
42. Semete B, Booysen L, Lemmer Y, Kalombo L, Katata L, Verschoor J, *et al*. *In vivo* evaluation of the biodistribution and safety of PLGA nanoparticles as drug delivery systems. Nanomedicine. 2010;6(5):662-671. DOI: 10.1016/j.nano.2010.02.002.
43. Xu H, Yang D, Cai C, Gou J, Zhang Y, Wang L, *et al*. Dual-responsive mPEG-PLGA-PGlu hybrid-core nanoparticles with a high drug loading to reverse the multidrug resistance of breast cancer: an *in vitro* and *in vivo* evaluation. Acta Biomater. 2015;16:156-168. DOI: 10.1016/j.actbio.2015.01.039.
44. Sánchez CA, Rodríguez E, Varela E, Zapata E, Páez A, Massó FA, *et al*. Statin-induced inhibition of MCF-7 breast cancer cell proliferation is related to cell cycle arrest and apoptotic and necrotic cell death mediated by an enhanced oxidative stress. Cancer Invest. 2008;26(7):698-707. DOI: 10.1080/07357900701874658.
45. Hwang KE, Na KS, Park DS, Choi KH, Kim BR, Shim H, *et al*. Apoptotic induction by simvastatin in human lung cancer A549 cells *via* Akt signaling dependent down-regulation of survivin. Invest New Drugs. 2011;29(5):945-952. DOI: 10.1007/s10637-010-9450-2.

46. Kotamraju S, Willams CL, Kalyanaraman B. Statin-induced breast cancer cell death: role of inducible nitric oxide and arginase-dependent pathways. Cancer Res. 2007;67(15):7386-7394. DOI: 10.1158/0008-5472.CAN-07-0993.
47. Ahn KS, Sethi G, Aggarwal BB. Simvastatin potentiates TNF-α-induced apoptosis through the down-regulation of NF-κB-dependent antiapoptotic gene products: role of IκBα kinase and TGF-β-activated kinase-1. J Immunol. 2007;178(4):2507-2516. DOI: 10.4049/jimmunol.178.4.2507.
48. Lopez S, Bermudez B, Montserrat-De La Paz S, Jaramillo S, Varela LM, Ortega-Gomez A, *et al*. Membrane composition and dynamics: a target of bioactive virgin olive oil constituents. Biochim Biophys Acta. 2014;1838(6):1638-1656. DOI: 10.1016/j.bbamem.2014.01.007.
49. Weijers RNM. Lipid composition of cell membranes and its relevance in type 2 diabetes mellitus. Curr Diabetes Rev. 2012;8(5):390-400. DOI: 10.2174/157339912802083531.
50. Leekumjorn S, Cho HJ, Wu Y, Wright NT, Sum AK, Chan C. The role of fatty acid unsaturation in minimizing biophysical changes on the structure and local effects of bilayer membranes. Biochim Biophys Acta. 2009;1788(7):1508-1516. DOI: 10.1016/j.bbamem.2009.04.002.
51. Chernomordik LV, Leikina E, Frolov V, Bronk P, Zimmerberg J. An early stage of membrane fusion mediated by the low pH conformation of influenza hemagglutinin depends upon membrane lipids. J Cell Biol. 1997;136(1):81-93. DOI: 10.1083/jcb.136.1.81.
52. Joardar A, Pattnaik GP, Chakraborty H. Combination of oleic acid and the gp41 fusion peptide switches the phosphatidylethanolamine-induced membrane fusion mechanism from a nonclassical to a classical stalk model. J Phys Chem B. 2022;126(20): 3673-3684. DOI: 10.1021/acs.jpcb.2c00307.
53. Joardar A, Pattnaik GP, Chakraborty H. Effect of phosphatidylethanolamine and oleic acid on membrane fusion: Phosphatidylethanolamine circumvents the classical stalk model. J Phys Chem B. 2021;125(48):13192-13202. DOI: 10.1021/acs.jpcb.1c08044.
54. Torchilin VP, Lukyanov AN, Klibanov AL, Omelyanenko VG. Interaction between oleic acid-containing pH-sensitive and plain liposomes:fluorescent spectroscopy studies. FEBS Lett. 1992;305(3):185-188. DOI: 10.1016/0014-5793(92)80663-2.